Journal of Hazardous Materials 201–202 (2012) 148–154

Contents lists available at SciVerse ScienceDirect

Journal of Hazardous Materials

journal homepage: www.elsevier.com/locate/jhazmat

Mechanochemical transformation of an organic ligand on mineral surfaces: The efficiency of birnessite in catechol degradation

Paola Di Leo[a,*], Maria Donata Rosa Pizzigallo[b], Valeria Ancona[c], Francesco Di Benedetto[d], Ernesto Mesto[e], Emanuela Schingaro[e], Gennaro Ventruti[e]

[a] Consiglio Nazionale delle Ricerche – Istituto di Metodologie per l'Analisi Ambientale, C.da S. Loja, Zona Industriale, 85050 Tito Scalo (PZ), Italy
[b] Dipartimento di Biologia e Chimica Agroforestale e Ambientale, Università di Bari Aldo Moro, Via Amendola 165/a, 70126 Bari, Italy
[c] Consiglio Nazionale delle Ricerche – Istituto di Ricerca sulle Acque, Via F. De Blasio 5, 70132 Bari, Italy
[d] Dipartimento di Chimica, Università di Firenze, Via della Lastruccia, 3, 50019 Sesto Fiorentino, Italy
[e] Dipartimento di Scienze della Terra e Geoambientali, Università di Bari Aldo Moro, Via Orabona, 4, 70125 Bari, Italy

ARTICLE INFO

Article history:
Received 5 September 2011
Received in revised form
15 November 2011
Accepted 16 November 2011
Available online 25 November 2011

Keywords:
Birnessite
Catechol
Mechanochemistry
Abiotic degradation

ABSTRACT

The aim of this work is to investigate the efficiency of the phyllomanganate birnessite in degrading catechol after mechanochemical treatments. A synthesized birnessite and the organic molecule were grounded together in a high energy mill and the xenobiotic-mineral surface reactions induced by the grinding treatment have been investigated by means of X-ray powder diffraction, X-ray fluorescence, thermal analysis and spectroscopic techniques as well as high-performance liquid chromatography and voltammetric techniques.

If compared to the simple contact between the birnessite and the organic molecule, mechanochemical treatments have revealed to be highly efficient in degrading catechol molecules, in terms both of time and extent. Due to the two phenolic groups of catechol and the small steric hindrance of the molecule, the extent of the mechanochemically induced degradation of catechol onto birnessite surfaces is quite high. The degradation mechanism mainly occurs via a redox reaction. It implies the formation of a surface bidentate inner-sphere complex between the phenolic group of the organic molecules and the Mn(IV) from the birnessite structure. Structural changes occur on the MnO_6 layers of birnessite as due to the mechanically induced surface reactions: reduction of Mn(IV), consequent formation of Mn(III) and new vacancies, and free Mn^{2+} ions production.

1. Introduction

The mechanochemical method, based on grinding reactants in solid phase, has recently aroused interest for its capability to degrade both organic [1–3] and inorganic [4] pollutants. When compared with other techniques, the mechanochemical method offers advantages for simple operations on a large amount of toxic compounds [3,5,6] by eliminating the use of organic solvent and facilitating the estimation of overall kinetic and thermodynamic parameters in the degradation processes. The direct contact between the mineral surface and the xenobiotic is indeed a crucial aspect of the mechanochemical interactions. In fact, it exerts a profound effect on the pathways and rates of chemical changes in organic pollutants and plays a primary role in activating surface reactions responsible for the abiotic degradation of organic pollutants without the presence of a solvent phase [3,6]. In order to fully exploit the potentials of the mechanochemical technique in remediating contaminated sites, a fundamental understanding at a molecular scale of organic molecule transformations onto mineral surfaces (i.e. individuation of the pathways of reactions) is still needed.

In the present study the capability of birnessite (δ-MnO_2) surfaces to mechanically degrade catechol has been investigated and the degradative mechanisms of the ligand onto the phyllomanganate has been hypothesized. To this purpose a synthesized birnessite and the organic ligand catechol were continuously grounded in a zirconia ball mill using different experimental setups. The phyllomanganate, its ground mixtures with the organic molecule, and their organic and aqueous extracts have been analyzed through several techniques.

The choice of birnessite as a substrate for mechanically induced degradation of the organic molecule catechol lies in the fact that the mineral possesses unique crystal-chemical characteristics [7–10] which confer it extensive redox and sorption properties. Besides, birnessite plays an important role in the fate of organic pollutants in soils because it is one of the most commonly identified Mn oxide

* Corresponding author. Tel.: +39 0971427234; fax: +39 0971427211.
E-mail address: pdileo@imaa.cnr.it (P. Di Leo).

0304-3894/$ – see front matter © 2011 Elsevier B.V. All rights reserved.
doi:10.1016/j.jhazmat.2011.11.054

minerals in soils and geochemical environments [11]. Birnessite is a layered phyllomanganate, i.e. a manganese oxide constituted by bidimensional layers of edge-sharing MnO_6 octahedra, with cations (K, Na, Li) in the interlayers and water molecules. These cations balance the negative charge arising from the layers as a consequence of the presence of Mn ions with an oxidation number lower than +4.

The organic molecule catechol, an ortho-diphenol, was chosen because it is commonly found in soils as an organic matter constituent (plant polyphenol), as an intermediate of microbial metabolism of xenobiotics, and is often used in laboratory experiments to model degradation of xenobiotics [12]. Further, ortho-type semiquinones are common intermediates in pesticide degradation pathways and are involved in oxidative coupling reactions leading to the formation of soil humic substances [13].

2. Materials and methods

2.1. Sample preparation and treatments

Catechol (hereafter CAT) was purchased from Aldrich Chemical Company (Milwaukee, WI, USA, 99% of purity) and used without a further purification. The phyllomanganate K-birnessite (*KBi*) was synthesized starting from $KMnO_4$ and HCl according to the method described by McKenzie [11].

CAT was mixed with synthesized *KBi* and 6.3 g of these mixtures (0.3 g of organic molecule + 6 g of phyllomanganate, 1/20 weight ratio) were grounded in a planetary ball mill. In the used mechanochemical reactor (Pulverisette-7, Frisch, Germany) – consisting of two zirconia pots with an inner volume of 45 cm^3 situated on a rotating disk – 14 zirconia balls (10 mm diameter) were arranged. The mill was operated applying a high rotation speed (700 rpm) for different milling times (4 steps of 15 min followed by 15 min cooling periods to prevent an excess of heating). Afterwards, ground mixtures were incubated at 30 °C in capped porcelain cups for periods ranging from 24 h to 7 d.

2.2. Solid phase analyses

Thermogravimetry (TG) and differential thermal analysis (DTA) curves were simultaneously recorded for the synthesized *KBi* using a thermal apparatus (SEIKO Instrument, UK), 10^5 μV DTA sensitivity, 10^7 μg TG sensitivity, under the following operating conditions: 20–25 mg sample weight, Al_2O_3 as a reference material, 20–1050 °C temperature range, 20 °C/min heating rate, nitrogen flow.

X-ray powder diffractometry (XRPD) was performed both on untreated birnessite and birnessite/CAT mixtures grounded for 60 min using a Philips PW1710 diffractometer with a conventional Bragg-Brentano parafocusing vertical geometry and a CuK_α radiation source, at the following operational conditions: 40 kV, 20 mA, 0.02° step scan, 10 s acquisition time per step.

X-ray photoelectron spectra (XPS) of untreated *KBi* and birnessite/catechol mixtures were collected using Theta Probe spectrometer (Thermo Electron Corporation), with a monochromatized AlK_α X-ray source, 400 μm spot size, 100 eV pass energy, under vacuum condition of 2×10^{-7} Pa in the analytical room. The sample was prepared as pressed pellets. The neutralization of sample charging was obtained using low energy electrons combined with Ar^+ ions and the binding energy scale was corrected using the signal of adventitious carbon (C*1s* = 284.8 eV).

Fourier transform infrared (FT-IR) spectra of untreated birnessite – at room temperature and heated for 1 h at 120 and 250 °C – and of 60-min ground birnessite/CAT mixtures have been acquired with a Nicolet 5 PC FT-infrared spectrometer using KBr pellets on a spectral range of 400–4000 cm^{-1}. Nominal resolution was 4 cm^{-1} and final spectra are the average of 128 scans.

Electron paramagnetic resonance (EPR) spectroscopy measurements have been performed at room temperature using a spectrometer (ER 200D-SRC, Bruker, Germany) operating at X-band (about 9.5 GHz). The *g*-values were determined using DPPH radical [2,2-di(4-tert-octyl-phenyl)-1-picrylhydrazyl, $g = 2.0037$] as an external standard. The measurements have been carried out on powdered samples of synthetic birnessite and birnessite/xenobiotic mixtures put in Teflon bags to avoid spurious effects from magnetic alignment phenomena and kept into amorphous silica capillaries. EPR parameters have been refined by means of spectral simulations.

X-ray fluorescence (XRF) analysis has been executed with an automatic spectrometer (PHILIPS PW1480, USA). The untreated birnessite was treated with elvacite solution (acetone 16%, w/v) and subsequently transformed in a pellet through a hydraulic press using a pressure of 10 tons. The loss of ignition (L.O.I.) was determined after heating the sample at 950 °C overnight.

2.3. Solvent extracts analyses

After each milling step and each incubation time, two aliquots of the milled and non-milled mixtures (50 mg) were extracted with 5 mL of aqueous solution and stirred at room temperature for 20 min. All the suspensions were centrifuged ($2880 \times g$) at 4 °C for 10 min. Then, the supernatants were filtered through 0.2 μm regenerated cellulose filters to determine (*i*) by high-performance liquid chromatography with diode-array detector (HPLC-DAD) the amount of un-reacted CAT and (*ii*) by anodic stripping voltammetry (ASV) the amount of Mn^{2+} ions possibly released as a consequence of the surface reactions of CAT with birnessite.

The HPLC analyses were performed with an apparatus from Perkin Elmer (Mod. 410, Monza, Italy) operating with a flow rate of 1 mL min^{-1}, a 3.9×150 mm C-18 column and the detector sets at 280 nm. The mobile phase, used in an isocratic elution, was composed of acidified water (0.05% phosphoric acid) and acetonitrile at a ratio of 20/80 (v/v). Standard solutions CAT were used as controls and all the experiments were performed in triplicate.

The concentration of manganese ions in solution was defined in alkaline aqueous solution ($Na_2B_4O_7$ + NaOH, pH 9.5–10) through ASV (Metrohm 693, Origgio, Italy) using the procedure Application Bulletin 123/3 (Metrohm Italiana). The metal reduction was obtained upon the hanging mercury drop electrode (HMDE). All the analytical determinations were repeated three times.

3. Results

The K and Mn concentrations in the synthesized birnessite have been measured from XRF analysis (*K* = 1.27 wt.% and Mn = 62.67 wt.%), whereas the water content has been estimated from the weight loss measured between 120 °C and 210 °C. The main features of DTA curve of the synthesized birnessite are represented by four endothermic peaks at about 100, 150, 790 and 830 °C and one exothermic peak at about 500 °C (Fig. 1). The two endothermic peaks at low temperature correspond to the loss of adsorbed and interlayer water, respectively. From the weight loss measured between 120 °C and 210 °C in TG curve [9] about a 7.39 wt.% of interlayer water has been deduced in the synthesized *KBi*. The exothermic peak at 500 °C corresponds to the transformation of the dehydrated birnessite to cryptomelane, whereas the endotherms at higher temperatures correspond to transformation into δ-Mn_2O_3 phase (~790 °C) and δ-Mn_2O_3 melting (~830 °C) [3].

The X-ray powder diffraction pattern of the *KBi* consists of a small number of broad lines (Fig. 2a), due to the low crystallinity of

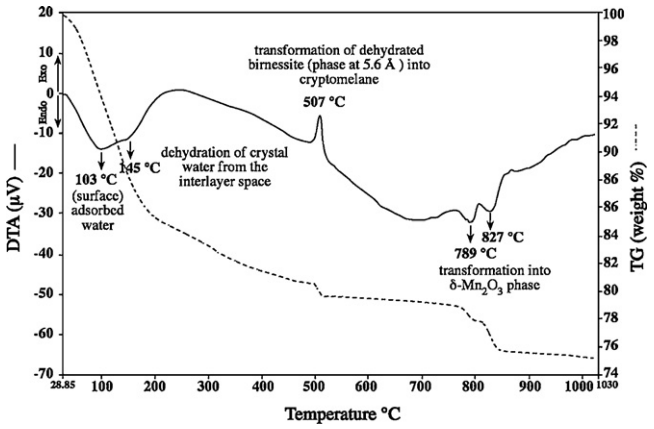

Fig. 1. Experimental TG–DTA curves of synthesized birnessite at room temperature and humidity.

the synthesized sample as well as to its being extremely fine grained (the submicron size of the particles could not be observed/resolved at the SEM scale) and defective for the strong occurrence of stacking faults in the structure [14–16]. This prevented an unambiguous derivation of the polytype, so that indexing of the experimental diffraction pattern was accomplished by assuming a simple, one layer (1*H*) polytype structure. The predominant peaks correspond both to the 0 0 1 reflection ($d_{(0\,0\,1)}$ = 7.25 Å) and 1 0 0 reflection ($d_{(1\,0\,0)}$ = 2.42 Å). The estimated lattice parameters of the compound are $a = b = 2.79$ Å and $c = 7.25$ Å. In 1*H* polytype, MnO_6 layers are superimposed one on top of the other [7,17] with about a 7 Å periodicity. The structural details of interlayer space are known to affect the crystal chemistry of birnessite [9]. In 1*H* polytype,

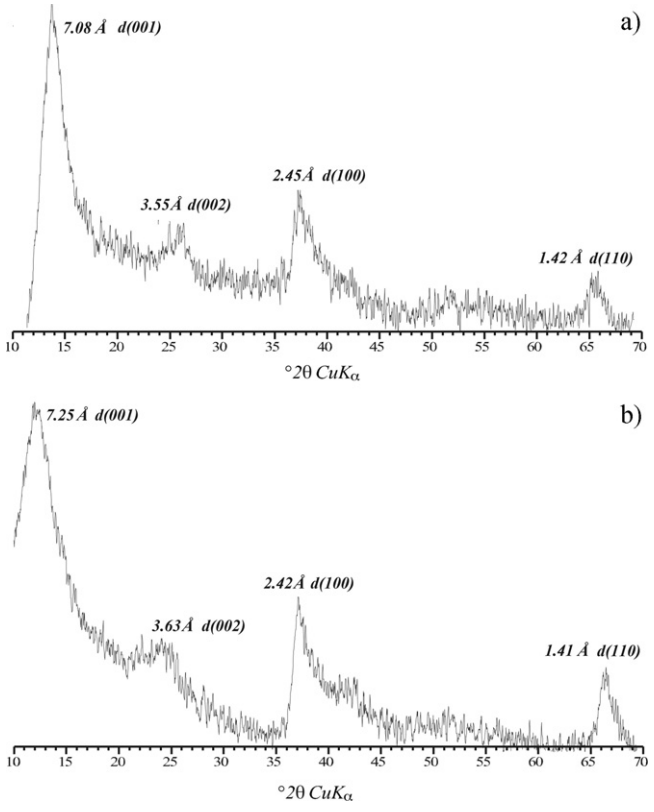

Fig. 2. Experimental X-ray powder diffraction patterns obtained for the (a) synthesized *KBi* at room temperature and humidity and for the (b) *KBi*–CAT mixture (1/20 weight ratio) mechanically ground for 60 min at room temperature.

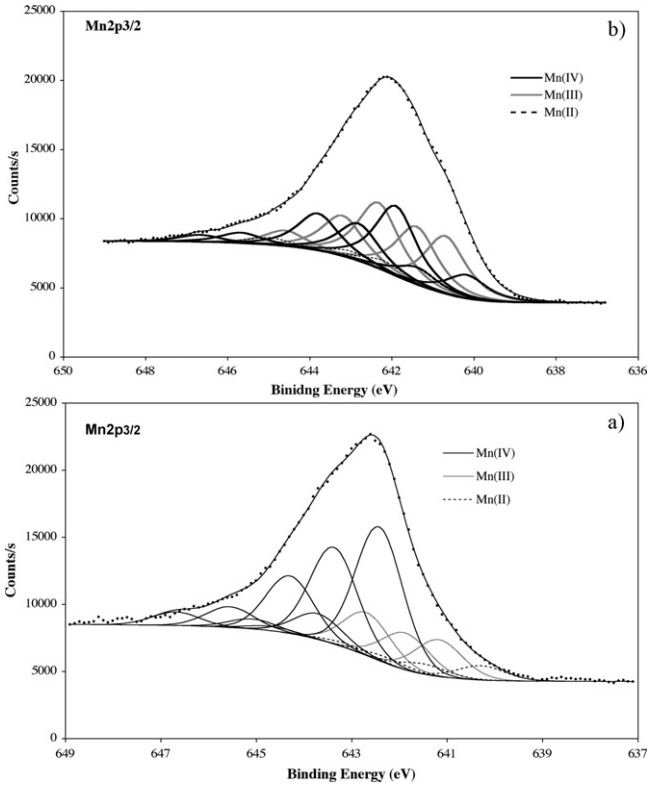

Fig. 3. Curve fitting of Mn($2p_{3/2}$) Shirley background subtracted spectra of (a) synthesized *KBi* and (b) *KBi*–CAT mixture (1/20 weight ratio) mechanically ground for 60 min at room temperature.

interlayer water molecules concur to the formation of two kinds of interlayer cavities: octahedral and prismatic ones with the oxygens of the upper and lower MnO_6 layers. No changes in the XRD pattern of synthesized birnessite were detected after 60 min grinding.

The synthesized *KBi* was also analyzed by XPS. The curve fitting of the Mn($2p_{3/2}$) peak was accomplished according to the procedure devised in Nesbitt and Banerjee [15]. Peaks were analyzed using Shirley background subtraction and a Gaussian–Lorentzian curve fitting algorithm. The results indicate the presence of three Mn species, amounting to about 8, 30, and 62% (atomic concentration) of Mn(II), Mn(III) and Mn(VI) respectively (Fig. 3a). Again no changes were observed by XPS spectroscopy in *KBi* after prolonged milling.

The EPR spectrum recorded for the untreated *KBi* (Fig. 4a) reveals the presence of a broad band, as expected for manganese species in solids. Due to the sensitivity of EPR to Mn^{2+} species the results indicate the occurrence of structurally bound Mn^{2+}. In fact, when the atoms are close enough, their magnetic fields interact and magnetic ordering swamps the fine EPR spectrum to yield a broad signal. On the other hand, isolated ions (>2 nm apart) yield a narrow 6-line spectrum due to magnetic hyperfine splitting [18,19].

FT-IR spectrum of *KBi* exhibits the typical broad band between 3500 and 3200 cm^{-1} due to the overlapping of the asymmetric and symmetric stretching modes of interlayer water molecules [9,20]. The band at 1626 cm^{-1} is relative to the bending mode of interlayer water molecules [9] and the one at 1436 cm^{-1} very likely arises from the adsorbed water on external grains, as it completely disappears after 1 h heating *KBi* at 250 °C (Fig. 5). The deconvolution of the 800–400 cm^{-1} region of the birnessite IR spectrum (Fig. 6a) revealed seven bands at 730, 670, 627, 578, 527, 480 and 440 cm^{-1}, corresponding to vibrational modes (wagging, bending and

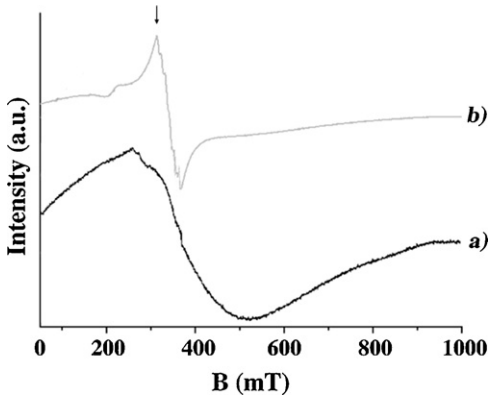

Fig. 4. Room temperature X-band EPR spectrum of a) untreated *KBi* and b) *KBi*–CAT mixture milled for 60 min. Magnetic field values are expressed in mT.

symmetrical and asymmetrical stretching vibrations of the octahedral layers in the birnessite structure) of Mn–O bonds [21].

Synthesized *KBi* was re-analyzed by powder XRD and XPS, EPR and FT-IR after 1 h of mechanochemical grinding with catechol.

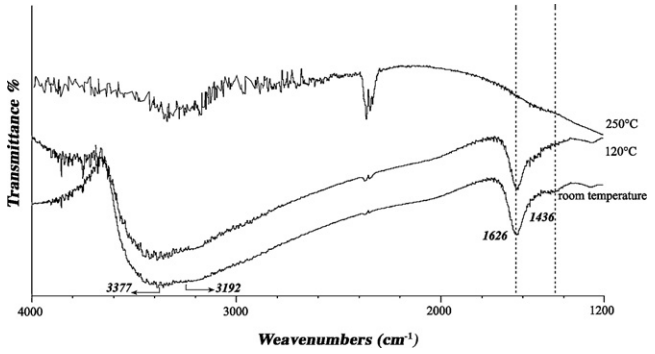

Fig. 5. IR spectrum of the synthesized *KBi* at room humidity and temperature and heated at 120 and 250 °C for 1 h.

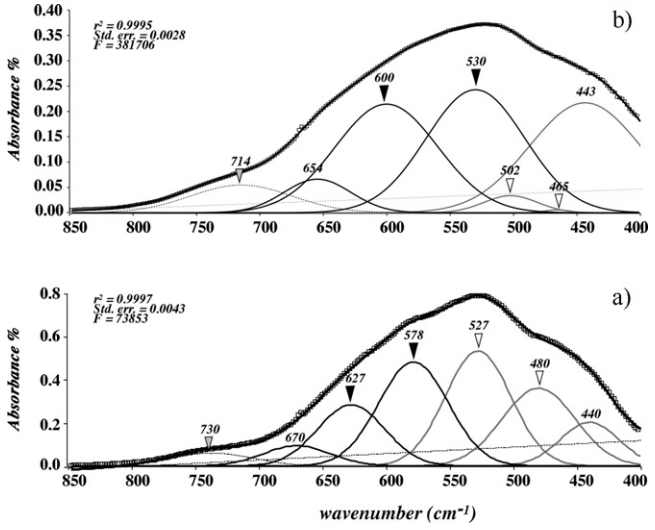

Fig. 6. IR spectra at room temperature and humidity. Deconvolution of the 800–400 cm^{-1} region showing the characteristic bands relative to the Mn-O stretching for (a) synthesized *KBi*, (b) *KBi*–CAT ground mixture. Triangles represent Mn–O stretching modes of the different Mn species: (▽) Mn(IV)–O, (▼) Mn(III)–O, and (▼) Mn–O within octahedra with only five shared edges instead of six. Curve fitting was achieved using PeakFit software, Jandel Scientific.

Mechanochemical grinding for 60 min causes severe changes in XRD and XPS, EPR and FT-IR.

The comparison between the XRD patterns of untreated *KBi* (Fig. 2a) and that relative to *KBi*–CAT (Fig. 2b) ground mixture evidences a shift of the prominent 001 peak towards lower *d* values, going from *KBi* ($d_{(001)}$ = 7.25 Å) to *KBi*–CAT ($d_{(001)}$ = 7.08 Å). This is indicative of an interlayer spacing reduction. On the other hand, the peak at $d_{(100)}$ = 2.42 Å of *KBi* is little shifted, within experimental error, to slightly higher *d* value (2.45 Å) in the *KBi*–CAT ground mixture.

The fitting of Mn($2p_{3/2}$) XPS spectrum of the treated birnessite (Fig. 3b) indicates a variation in the relative population on Mn species: about 14, 51, and 35% of Mn(II), Mn(III), and Mn(IV), respectively, was found. This clearly indicates that grinding birnessite with CAT promotes reduction of structural Mn(IV), and a consequent increase of both Mn(III) and Mn(II) species. However, the extent of Mn(II) production is negligible if compared to that of Mn(III) species. Further, water is also produced from the degradative reaction of CAT molecules at birnessite surfaces.

The EPR spectrum of mechanically treated mixture depicts the characteristic six-line pattern of the isolated Mn^{2+} species (Fig. 4, curve b), besides the obvious presence of the superimposed broad band due to "structural" Mn^{2+} previously described. A second signal appears in spectrum of the ground birnessite–catechol mixture (Fig. 4, black arrow in curve b), perfectly superimposed to the six-lines ones, which clearly indicates that the free Mn^{2+} species are present in a large amount [18].

The MnO stretching region between 400 and 850 cm^{-1} underwent several changes after the phyllomanganate was grounded for 60 min with CAT (Fig. 6b). These changes evidence a relative reduction of the band assigned to Mn(IV)–O stretching vibrations with respect to the ones assigned to Mn(III)–O, in agreement with XPS results which also indicate a decrease in the absolute concentration of Mn(IV) and an increase of Mn(III) species.

Infrared spectra of *KBi*–CAT mixture, in the range of 1600–1400 cm^{-1}, evidence the formation of catechol by-end products. The presence of two bands at 1587 and 1395 cm^{-1} are indicative of reaction products, which can be hypothesized to be re-adsorbed onto birnessite surfaces (Fig. 7a and b). The 1587 cm^{-1} band can be attributed to the skeletal ring bonding modes corresponding to the C=C double bond *in-plane* vibrations of the aromatic ring in simple and polycyclic aromatics, including quinones [22,23]. The band at 1395 cm^{-1} can be assigned to COO^- groups [24] as well as to the bending vibration of CH groups [25]. Both bands (1587 and 1395 cm^{-1}) are compatible with the formation of a semi-quinone as a by-end product of the redox reaction at the birnessite surfaces.

High-performance liquid chromatography allowed us to estimate the amount of un-reacted CAT after grinding with birnessite and the anodic stripping voltammetry to detect the amount of Mn^{2+} ions possibly released as a consequence of the surface reactions of CAT with birnessite. The difference between the quantity of the organic molecule in methanolic extracts of ground *CAT–KBi* mixtures and the control tests, expressed as percentage (hereafter removal %), represents the estimation of the *KBi* ability in removing CAT by means of mechanochemical treatments. This seems to be quite high: CAT removal by *KBi* is >90% after the first 15 min of milling (Fig. 8). At this time, the amount of Mn^{2+} released from *KBi* structure is also quite high, although the maximum liberation of Mn^{2+} form the structure (about 286.3 μmol; Fig. 9) is obtained after 60 min of milling time, and did not change during the following time of incubation. For a contact between *KBi* and CAT molecules with no grinding, 60 min are needed to get the 60% of CAT removal. An almost total sequestration of the CAT is obtained for 24 h of incubation after grinding (Fig. 8).

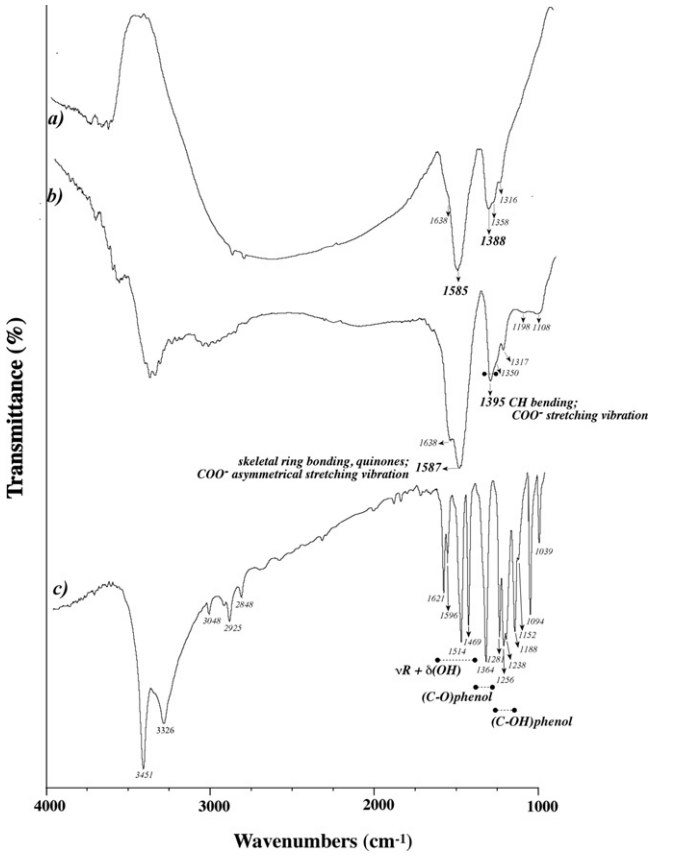

Fig. 7. Birnessite-subtracted IR spectra of *KBi*–CAT mixtures ground for 30 min a) and 60 min b). All spectra have been recorded at room temperature and humidity. Solid CAT IR spectrum c) with assigned bands is also reported.

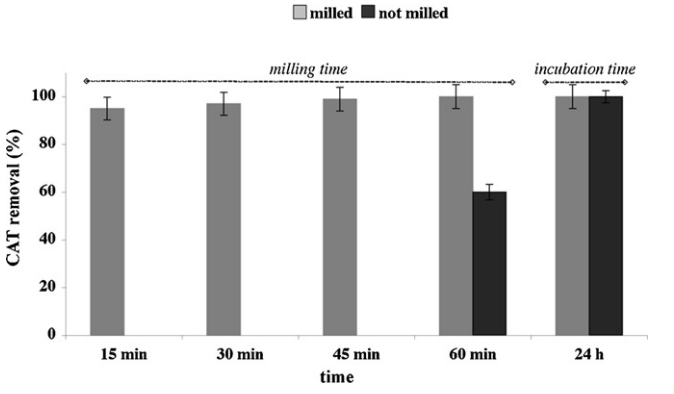

Fig. 8. Catechol removal (%) from milled and not-milled *KBi*–CAT mixtures (1/20 xenobiotic/oxide weight ratio) for different times. Errors bars represent standard deviations.

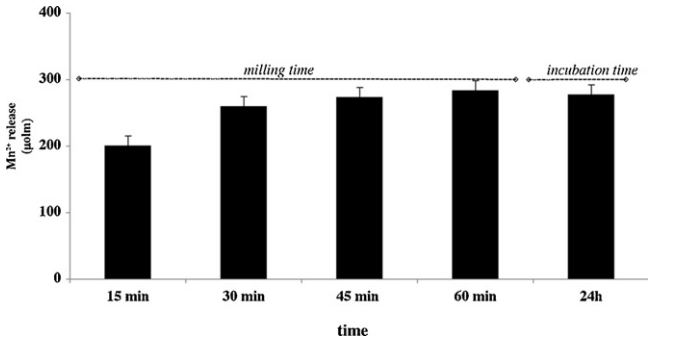

Fig. 9. Concentration of Mn^{2+} ions (μmol) in extracts from *KBi*–CAT ground mixtures (1/20 xenobiotic/oxide weight ratio). Error bars represent standard deviations.

4. Discussion

In order to test the efficiency of birnessite in degrading catechol by mechanical milling as well as get a fundamental comprehension of the surface reactions at the base of its possible abiotic degradation, synthesized *KBi*, synthesized *KBi*–organic molecule mixtures and their solvent extracts were analyzed. X-ray powder diffraction and spectroscopic techniques (infrared spectroscopy and the surface sensitive technique XPS) were used to detect changes occurring in the structure of the birnessite as a consequence of the prolonged milling with the organic molecule. Infrared spectroscopy has also been used to characterize the "by-end products" of CAT. EPR spectroscopy was used to monitor the possible liberation of Mn^{2+} species from birnessite structure induced by surface interaction with the organic ligand CAT during mechanochemical treatments. Besides, the ability of *KBi* to remove catechol molecules by means of mechanochemical treatments was estimated by using HPLC and ASV allowed us to detect the amount of Mn^{2+} ions possibly released as a consequence of the surface reactions of CAT with birnessite.

Combining XRF, TG–DTA, XPS results made it possible to calculate the following structural formula for the synthesized *KBi* used in the mechanochemical treatments with CAT:

$$K_{0.03}Mn_{0.08}^{2+}Mn_{0.11}^{3+}(Mn_{0.62}^{4+}Mn_{0.19}^{3+}\square_{0.19})O_{1.57}(OH)_{0.43}\cdot 0.39H_2O,$$

in which the symbol □ corresponds to vacant layer sites.

The presence of an appreciable amount of Mn^{3+} (about 30% of total Mn) in the *KBi* synthesized in the present work bears evidence that the reduction during synthesis does not stop at Mn^{4+} production [15]. Mn^{3+} is probably reduced at the surface of precipitated birnessite crystals, where it is available to be uptaken into the solid. Its low solubility probably prevents it from being released to solution, thus promoting its incorporation into the *KBi* structure both in the interlayer space ($Mn_{interlayer}$, [8,9]) and the manganese (MnO_6) layers [7]. In addition, mixed manganese valence state is quite common in birnessite [7–17]. Indeed, large monovalent cations (which occupy the ditrigonal prismatic interlayer sites) together with Mn(III) and Mn(II) cations (present in octahedral interlayer cavities) charge balance Mn(IV) and/or vacant octahedra in the MnO_6 layers of the mineral. Mn(III) cations have also been reported to occupy protruding interlayer octahedra which share one face with adjacent vacant sites in MnO_6 layers (the so called $Mn_{interlayer}$ [8]). Usually, Mn(III) distribution in protruding octahedra is disordered and play a major role in polytype formation.

EPR strongly supports the incorporation of the Mn^{2+} species into the structure of *KBi*: the EPR signal recorded for the untreated *KBi* (Fig. 1a) also establishes that the Mn^{2+} ions are close enough to structural manganese to order magnetically [18,19]. However, the Mn^{2+} species detected in *KBi* (about 8% of total Mn as deduced by XPS; see Section 3), being this ion 45% larger than Mn^{4+} [20], are unlikely to substitute for Mn(IV) at octahedral layer site. Therefore, its presence in the structure of the synthesized *KBi* has to be restricted only to surface and/or interlayer positions [15,16].

Potter and Rossman [21] noted that the broadening of structural modes in the infrared spectra is not related to disorder measured by XRD and is more sensitive to local differences in bonding environments. These local differences for the octahedral layer include a range in the number of shared edges of the Mn octahedra due to vacancies in the Mn octahedral layer sites or local disordering of the structure, and may also reflect variation in the Mn–O distances due to the presence of Mn^{3+} or Mn^{2+} in the octahedral layer structure or interlayer region [26,27]. The wide range of oxidation state of the Mn in birnessite interlayer region [7,17] could contribute

to the broadened absorption features in the 350–800 cm^{-1} region. The observed broadness of IR bands for *KBi* in the 800–400 cm^{-1} region (Fig. 6a) is clearly a consequence of the wide distribution in the birnessite of metal–oxygen distances as a consequence of the different oxidation states exhibited by manganese [7–9,26].

The deconvoluted bands in the 800–400 cm^{-1} region have been interpreted as due to Mn(IV)–O and Mn(III)–O vibrational modes. Specifically, the prominent infrared bands located at 480 and 527 cm^{-1} could mainly arise from the Mn(IV)–O stretching modes. Highly crystallized stoichiometric K-birnessite – mainly Mn(IV) in octahedral positions – exhibits in fact prominent and sharp bands at 513 and 478 cm^{-1} [28,29] and at 510 and 470 cm^{-1} [21]. The other two broad bands occurring at lower frequencies in the FT-IR spectrum of *KBi* (578 and 627 cm^{-1}; Fig. 6a) could likely correspond to the Mn–O stretching of the Mn(III) species. The vacancies in the Mn oxide layers of synthesized *KBi* result in Mn octahedra with only five shared edges instead of six. This could be responsible for the additional Mn–O stretching mode at about 730 cm^{-1} observed in the infrared spectrum of birnessite [30]. The broadness of 440 cm^{-1} band is indeed evidence of the poorly crystalline order of the synthesized birnessite [21,28].

The efficiency of mechanochemical treatments in removing CAT molecules in presence of the highly reactive phyllomanganate birnessite and without using organic solvents is quite high. If compared to a simple contact between synthesized birnessite and organic molecule (incubation without milling), the mechanochemical treatments likely increase the removal efficiency of *KBi* for catechol, both in terms of time and extent. The almost complete removal of CAT molecules is quite rapid. After only a 5-min grinding treatment the 100% of CAT molecules is removed by the synthesized phyllomanganate, whereas to remove the same amount 24 h of incubation without milling are needed.

The mechanochemical treatments of *KBi* with CAT molecules yield to a large decrease in the concentration of Mn(IV) species in the MnO_6 layers, and a consequent increase in Mn(III) species (see Figs. 3b and 6b). These results are consistent with the observed variation in the diffraction pattern of *KBi*–CAT mixture. An increase in Mn(II), Mn(III) concentration in the interlayer might be responsible for the shrinking of the 0 0 1 spacing observed in *KBi*–CAT pattern [28,31]. A concomitant water removal may result in the observed shortening of interlayer spacing [31]. A combination of Mn(III) and/or vacancy substitutions for Mn(IV) in MnO_6 layer may account for the slight shift of the 1 0 0 reflection towards higher values, which points to a lateral enlargement of MnO_6 layer. On the other hand, the mechanochemical treatment also induces the release of Mn^{2+} from birnessite structure as a consequence of catechol oxidation. XPS results indicate that the oxidative mechanism of CAT by birnessite surfaces involves the production of Mn^{2+} species (Fig. 3). Besides, the spectral features of the EPR Mn^{2+} signals in *KBi*–CAT ground mixture (in particular the mean hyperfine splitting of the sextet, 9.6 mT; Fig. 4, curve b) confirm that the Mn^{2+} species are isolated from the structure, likely coordinated by water molecules in a more or less distorted octahedral arrangement [32]. The linewidth value (3.5 mT) evidences an inhomogeneous broadening of the line due to a locally disordered arrangement but indicates that the broadening effects due to the concentrated magnetic environment – and provided by the bulk of *KBi* – are limited on the Mn^{2+} EPR signal. What observed is conceivable only if the mean distance between manganese ions is large (>2 nm apart [18]), thus suggesting that the Mn^{2+} species produced by the mechanically induced oxidative mechanism of CAT molecules onto birnessite surfaces can no more be considered structurally bound to *KBi* lattice. Indeed, solvent extract analyses by ASV also evidenced that the degrading mechanism of the organic molecule by birnessite surfaces induces the release of Mn^{2+} into solution. The maximum liberation of Mn^{2+} from the structure (about 286.3 μmol) is obtained after 60 min of milling time (see Fig. 9). Accordingly, the production of free Mn^{2+} (i.e. larger release of Mn^{2+} ions from the phyllomanganate structure) can be considered large in the case of the birnessite mechanochemical treatment with CAT. This is therefore compatible with an oxidative reaction of CAT molecules at birnessite surfaces.

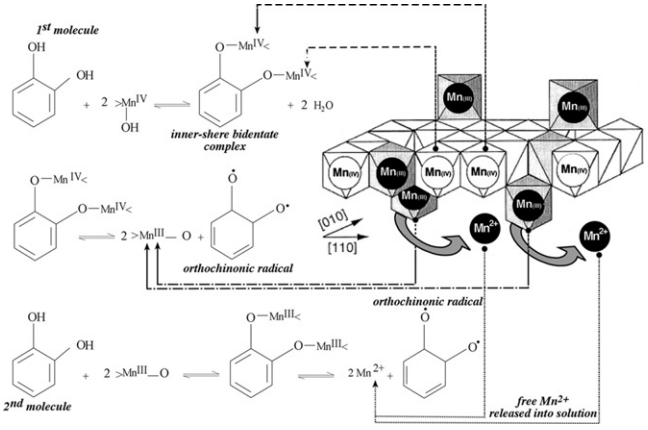

Fig. 10. Surface reaction mechanism of CAT molecules at birnessite surfaces after mechanochemical interactions.

According to IR results, the oxidation of CAT molecules occurs at the birnessite surfaces and leads to the formation of a semiquinone as a "by-end product" of the redox reaction (see Fig. 7a and b). On the other hand, XRD and spectroscopy results support the idea that the degradative reaction of CAT molecules at the surfaces of birnessite mainly involves the Mn sites in which Mn(IV) cations are localized at the centers of the octahedra from the MnO_6 layers. As the CAT oxidation proceeds Mn(III) and Mn(II) species are indeed produced at the expense of the structural Mn(IV). The latter is firstly reduced to Mn(III), then to surface/interlayer Mn(II), and finally released from the structure as Mn^{2+}.

5. Catechol reaction mechanism at birnessite surfaces

Integrating information from different techniques on solid-phase and comparison with batch-type experiments from previous studies [24,33] made it possible to get a comprehensive picture of the most reliable reaction mechanism of degradation of CAT molecules onto *KBi* surfaces, thus allowing the individuation of specific sites in the synthesized oxides on which catechol molecules were preferentially adsorbed, and thus degraded. X-ray diffraction and spectroscopy results suggest that CAT are mainly adsorbed onto the Mn_{layer} sites of birnessite – i.e. the MnO_6 octahedra from the layers at the center of which an Mn(IV) is located – and the reaction mechanism implies the formation of the Mn(III) and free Mn^{2+} ions production.

The hypothesized degradative mechanism, as sketched in Fig. 10, also implies the formation of a surface inner-sphere bidentate complex with Mn(IV) in the Mn_{layer} sites – i.e. the Mn(IV) centered at layer MnO_6 octahedra – of the birnessite structure. Subsequently, the transfer of the two electrons from the organic molecule to two structural Mn forms an orthochinonic radical and two Mn(III). A following step of the reaction would involve another catechol molecule to form a new complex with Mn(III) from birnessite: the oxidative reaction would produce a simultaneous release of two Mn^{2+}. The proposed mechanism is in accordance with a possible increase in interlayer water content. Indeed, each step implies the formation of two water molecules. Because of oxidative coupling, newly-formed radicals keep reacting to transform into quinonic, dimeric and/or polymeric molecules. The extent of the degradation of CAT onto birnessite surfaces is very high for the

organic molecule. This is likely a consequence of the two phenolic groups of catechol.

Acknowledgements

The authors wish to acknowledge the Tuscan Regional Administration and the Department of Chemistry (University of Florence) for providing funds for the use of EPR instruments. Prof. M. Romanelli, from the University of Florence, is kindly acknowledged both for his help in the acquisition of EPR spectra and the useful discussions. Prof. P. Ruggiero and Prof. F. Scordari, from the University of Bari, are also kindly acknowledged for their useful comments and discussions.

References

[1] V.V. Boldyrev, K. Tkáčová, Mechanochemistry of solids: past, present, and prospects, J. Mater. Synth. Process. 8 (2000) 121–132.
[2] S. Yariv, I. Lapides, The effect of mechanochemical treatments on clay minerals and mechanochemical desorption of organic material onto clay minerals, J. Mater. Synth. Process. 8 (2000) 223–233.
[3] A. Napola, M.D.R. Pizzigallo, P. Di Leo, M. Spagnuolo, P. Ruggiero, Mechanochemical approach to remove phenanthrene from a contaminated soil, Chemosphere 65 (2006) 1583–1590.
[4] S. Montinaro, A. Concas, M. Pisu, G. Cao, Remediation of heavy metals contaminated soils by ball milling, Chemosphere 67 (2007) 631–639.
[5] A. Nasser, G. Sposito, M.A. Cheney, Mechanochemical degradation of 2, 4-D adsorbed on synthetic birnessite, Colloids Surf. A 163 (2000) 117–123.
[6] M.D.R. Pizzigallo, P. Di Leo, V. Ancona, M. Spagnuolo, E. Schingaro, Effect of aging on catalytic properties in mechanochemical degradation of pentachlorophenol by birnessite, Chemosphere 82 (2011) 627–634.
[7] B. Lanson, V.A. Drits, E. Silvester, A. Manceau, Structure of H-exchanged hexagonal birnessite and its mechanism of formation from Na-rich monoclinic buserite at low pH, Am. Mineral. 85 (2000) 826–838.
[8] B. Lanson, V.A. Drits, A. Gaillot, E. Silvester, A. Plançon, A. Manceau, Structure of the heavy-metal sorbed birnessite: Part 1. Results from X-ray diffraction, Am. Mineral. 87 (2002) 1631–1645.
[9] A.C. Gaillot, D. Flot, V.A. Drits, A. Manceau, M. Burghammer, B. Lanson, Structure of synthetic K-rich birnessite obtained by high-temperature decomposition of $KMnO_4$: I. Two-layer polytype from 800 °C experiment, Chem. Mater. 15 (2003) 4666–4678.
[10] A.C. Gaillot, V.A. Drits, A. Manceau, B. Lanson, Structure of synthetic K-rich birnessite obtained by high-temperature decomposition of $KMnO_4$, substructures of K-rich birnessite from 1000 °C experiment, Microporous Mesoporous Mater. 98 (2007) 267–282.
[11] R.M. McKenzie, The synthesis of birnessite, cryptomelane and some other oxides and hydroxides of manganese, Miner. Mag. 38 (1971) 493–502.
[12] J.P. Martin, K. Haider, L.F. Lin, Decomposition and stabilization of ring ^{14}C-labeled catechol in soil, Soil Sci. Soc. Am. J. 43 (1979) 100–104.
[13] B.I. Escher, M. Snozzi, R.P. Schwarzenbach, Uptake, speciation, and uncoupling activity of substituted phenols in energy transducing membranes, Environ. Sci. Technol. 30 (1996) 3071–3079.
[14] S.E. Fendorf, D.L. Sparks, J.A. Franz, D.M. Campioni, Electron paramagnetic resonance stopped-flow kinetic study of manganese(II) sorption-desorption on birnessite, Soil Sci. Soc. Am. J. 57 (1993) 57–62.
[15] H.W. Nesbitt, D. Banerjee, Interpretation of XPS Mn(2p) spectra of Mn oxyhydroxides and constraints on the mechanism of MnO_2 precipitation, Am. Mineral. 83 (1998) 305–315.
[16] E. Silvester, A. Manceau, V.A. Drits, Structure of synthetic monoclinic Na-rich birnessite and hexagonal birnessite: II. Results of chemical studies and EXAFS spectroscopy, Am. Mineral. 82 (9–10) (1997) 962–978.
[17] V.A. Drits, E. Silvester, A.I. Gorshkov, A. Manceau, Structure of synthetic monoclinic Na-rich birnessite and hexagonal birnessite: I. Results from X-ray diffraction and selected-area electron diffraction, Am. Mineral. 82 (1997) 946–961.
[18] J.E. Amonette, R.K. Kukkadapu, A.S. Lea, C.J. Matocha, D.L. Sparks, W.F. Bleam, S.J. Yoon, Electron Paramagnetic Resonance studies of mineral surface chemistry, Environmental Dynamics and Simulation (1999) Annual Report, pp. 3–18.
[19] H.T. Zhu, J. Luo, H.X. Yang, J.K. Liang, G.H. Rao, J.B. Li, Z.M. Du, Birnessite-type MnO_2 nanowalls and their magnetic properties, J. Phys. Chem. 112 (2008) 17089–17094.
[20] O. Prieto, M. del Arco, V. Rives, Structural evolution upon eating of sol-gel prepared birnessite, Thermochim. Acta 401 (2003) 95–109.
[21] M.R. Potter, G.R. Rossman, The tetravalent manganese oxides: identification, hydration, and structural relationships by infrared spectroscopy, Am. Mineral. 64 (1979) 199–1218.
[22] L.J. Bellamy, The Infra-red of Complex Molecules, third ed., Chapman and Hall, London, 1975.
[23] A. Naidja, P.M. Huang, J.M. Bollag, Comparison of reaction products from the transformation of catechol catalysed by birnessite or tyrosinase, Soil Sci. Soc. Am. J. 62 (1998) 188–195.
[24] J. Niemeyer, Y. Chen, J.M. Bollag, Characterization of humic acids, composts and peat by diffuse reflectance Fourier-transform infrared spectroscopy, Soil Sci. Soc. Am. J. 56 (1993) 135–140.
[25] W.V. Gerasimovicz, D.M. Byler, H. Susi, Resolution enhanced FT-IR spectra of soil constituents: humic acid, Appl. Spectrosc. 40 (1986) 504–507.
[26] R.D. Shannon, Revised effective ionic radii and systematic studies of interatomic distances in halides and chalcogenides, Acta Crystallogr. (1976) 751–767.
[27] J.E. Post, D.R. Veblen, Crystal structure determinations of synthetic sodium, magnesium, and potassium birnessite using TEM and the Rietveld method, Am. Mineral. 75 (1990) 477–489.
[28] C. Julien, M. Massot, C. Poinsignon, Lattice vibrations of manganese oxides: Part I. Periodic structures, Spectrochim. Acta Part A 60 (2004) 689–700.
[29] L.X. Yang, Y.J. Zhu, G.F. Cheng, Synthesis of well-crystallized birnessite using ethylene glycol as a reducing reagent, Mater. Res. Bull. 42 (2007) 159–164.
[30] E.A. Johnson, J.E. Post, Water in the interlayer region of birnessite: importance in cation exchange and structural stability, Am. Mineral. 91 (2006) 609–618.
[31] Kh.S. Abou-El_Sherbini, M.H. Askar, R. Schöllhorn, Hydrated layered manganese dioxide: Part I. Synthesis and characterization of some hydrated layered manganese dioxides from α-$NaMnO_2$, Solid State Ionics 150 (2002) 407–415.
[32] B.A. Goodman, J.B. Raynor, Electron Spin Resonance of transition metal complexes, in: H.J. Emelens, A.G. Sharpe (Eds.), Advances in Inorganic Chemistry and Radiochemistry, Academic Press, New York, 1970, pp. 135–361.
[33] C.J. Matocha, D.L. Sparks, J.E. Amonette, R.K. Kukkadapu, Kinetics and mechanism of birnessite reduction by catechol, Soil Sci. Soc. Am. J. 65 (2001)58–66.